Research Paper

DESIGN AND SIMULATION OF ACTIVE SINGLE-AXIS PHOTOVOLTAIC TRACKER FED PERMANENT MAGNET BRUSHLESS MOTOR FOR COMMERCIAL APPLICATIONS

Sathishkumar Shanmugam[1] Meenakumari Ramachandran[2] Anbarasu Loganathan[3]

Address for Correspondence

[1]Research Scholar Anna University, Chennai & Assistant Professor, Department of EEE, Jansons Institute of Technology, Coimbatore.

[2]Professor, Depertment of EEE, Kongu Engineering College, Erode

[3] Assistant Professor, Department of EEE, Erode Sengunthar Engineering college, Erode.

ABSTRACT—

This Research paper presents the modelling and simulation of an active single axis solar tracker fed permanent magnet (PM) brushless motor for residential applications. The aim of this work is to extract the maximum available energy from the sun by tracking its irradiance through some mechanical means as well as to feed the energy to the permanent magnet brushless motor for consumer appliances. A photovoltaic module with sun tracking arrangement by means of a Permanent Magnet Direct Current (PMDC) motor is proposed. The solar irradiance is detected by two Light-Dependent Resistor (LDR) sensors that are located on the top and bottom surface of the photovoltaic panel. The position and status of the sun are detected and the resultant signals from the sensors are fed into an electronic control system that operates a low-speed tracking motor to rotate the panel. Based on the sensor signals, the microcontroller determines the optimum angle for the panel to track at various insolation. A battery with charge controller topology is used to store the electrical energy generated from the sun. Then the stored energy is given to the three phase inverter driven ceiling fan motor. A computer model of the standalone solar tracker system feeding ceiling fan is modelled using MATLAB/Simulink environment.

KEYWORDS—Irradiance, Smart PV Tracker, LDR Sensor, PMDC Motor, Ceiling Fan PM Brushless Motor.

INTRODUCTION

The world population is increasing day by day and the demand for energy is increasing accordingly. Oil and coal as the main source of energy nowadays, is expected to end up from the world during the recent century which explores a serious problem in providing the humanity with an affordable and reliable source of energy. The need of the hour is renewable energy resources with cheap running costs. Among the renewable energy resources, solar energy is the most essential and sustainable energy because of its abundance and sustainability. Irrespective of the sunlight's intermittency, solar energy is widely available and completely free of cost. Recently, Photovoltaic (PV) system is well recognized and widely utilized to convert the solar energy for electric power applications. It can generate Direct Current (DC) electricity without environmental impact and emission by way of solar radiation. The DC power is converted to Alternating Current (AC) power with an inverter, to power local loads or fed back to the utility.

MODELING OF SMART PV TRACKER

A solar tracker is a device that orient photovoltaic array towards the sun. In flat-panel PV applications trackers are used to minimize the angle of incidence between the incoming light and a photovoltaic panel. This increases the amount of energy produced by the photovoltaic array. The main focus in this section is to simulate the single axis solar tracking system during the automatic mode using MATLAB^{TM} /Simulink^{TM}. The simulation run was performed in every second of the entire 10 hours or 36000 seconds of experimental set up. The ODE45 solver type of variable step size was used throughout the simulations.

The simulation model is implemented in a way that when the sun irradiance falls on the sensors, the PMDC motor moves the PV panel in an incremental way till the sunset. The LDR sensors signal provide the input to the microcontroller for the PMDC motor to rotate the PV panel. The charging and discharging mechanism of the battery uses the charger subsystem. The PV tracking panel with the two LDR sensors generates the voltage outputs (i.e. V_LDR_B and V_LDR_T) based on the corresponding sun irradiance data used in the simulation. The irradiance from the sun model was obtained by dividing the power obtained from the tracker by the surface area of the PV cells. The PMDC motor rotates the panel at an angle based on the microcontroller PWM signal. This process repeats again until the sunset. During the process, the PV panel generates direct current that keeps the 12V battery charged. The battery gets charged or discharged depending on the state of the charger.

SMART TRACKER PV PANEL

The smart tracker panel was installed with two LDR sensors. Assuming both sensors are placed in parallel with the PV panel, the effective irradiance is similar. As the results, the smart tracker is unable to perform the proposed sun tracking algorithm. To circumvent this, the top and bottom sensors were positioned at 45° and 135° respectively as seen in Fig.1. When the sunlight falls onto the PV panel, the LDR sensors generate different voltages (that is V_LDR_B and V_LDR_T according to the changes in the sun irradiance) to move the PV panel.

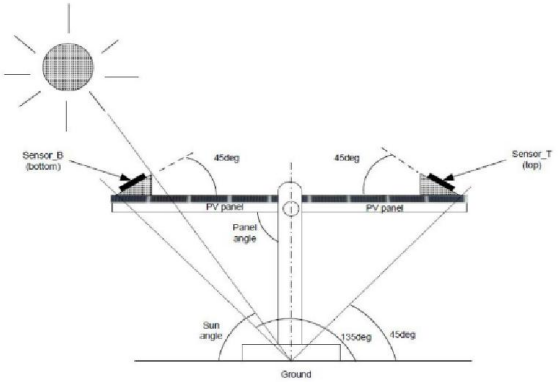

Fig.1 PV Panel and LDR Sensor Angle Position

MICROCONTROLLER MODEL

As shown in Fig.2, the microcontroller model is modeled using the embedded MATLAB^{TM} function. The inputs to this function are LDR_B and LDR_T, a real time clock and initial buffer value of 1.5. One of the inputs (named Extime) is used to compare the current time with the previous time when the PWM

value changes. The microcontroller generates output duration of 1.5ms to rotate the PV panel if the voltage difference of the LDR sensors is less than 0.07V and are both less than 0.75V (very low irradiance).

If LDR sensors voltages are both greater than 0.75V but the voltage difference is less than 0.07V, the PV panel remains in the current position. In the case when the LDR sensor values is greater than 0.07V, the motor turns the PV panel by adjusting its PWM value until the sensors' voltages are equal. The next cycle starts after the delay time of 0.7 seconds during the simulation.

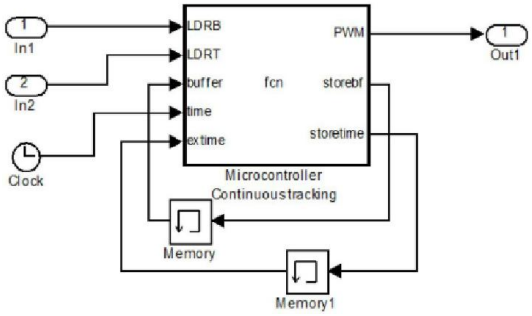

Fig.2 Microcontroller Model

The process flow chart for the microcontroller operation is illustrated in Fig.3 below.

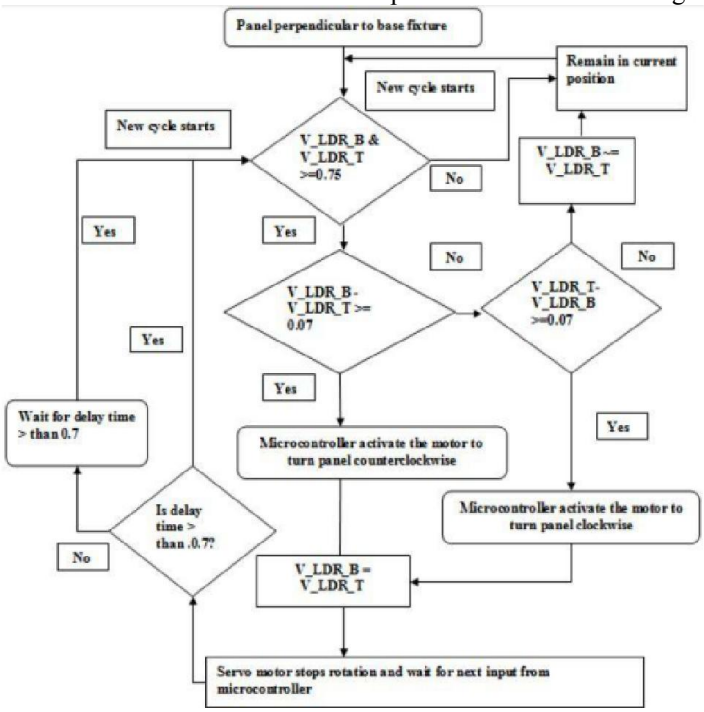

Fig.3 Process Flow Chart for Microcontroller Operation

MOTOR MODEL

The solar panel is designed to drive the PV panel in a small angle, between 0 to 180 degrees at a low speed. PWM is used to control the motor. The PWM is a continuous square wave with a period of 20ms. With the PWM signal, the output shaft of the PMDC motor changes the angular position of the PV panel. The following parameters are used to model the PMDC motor.

1. Moment of inertia (J) = 0.01 kg.m^2
2. Damping ratio (B) = 0.1 Nm.s
3. Electromotive force constant (K_t) =0.01Nm/Amp
4. Back electromotive force constant (K_e) =0.01V/rad/s
5. Electric resistance (R_m) = 1 ohm
6. Electric inductance (L_m) = 0.5 H
7. Input Voltage (V_m)
8. Output angle (θ)

As the modeling of the PMDC motor is common, we write the following transfer function between the output rotational angle and the input voltage is written as follows,

$$\frac{\theta(s)}{V_m(s)} = \frac{1}{s}\left[\frac{K_t}{(Js+B)(L_m s+R_m)+K_t K_e}\right] \quad (1)$$

Based on this transfer function, the PMDC motor model can be modeled in Simulink using the look-up tables. The lookup table uses the PWM as an input to rotate the motor to a pre-determined angle. When pulse width changes from 1.25ms to 1.75ms, the panel angle changes from 0 degree to 180 degree in a linear manner. As the PWM values and its corresponding angles are incorporated in the look-up tables, the panel angle variation is linear thereby avoiding non-linearty. The actual and the desired pulse-width are then compared to obtain the error signal for the Proportional- Integral-Derivative (PID) controller (using the controller gains: K_p=60, K_i=30, K_d=3) to drive the motor to the desired angle. The embedded MATLAB^{TM} function block is used to deactivate the motor load when it is not turning. An external load of pure resistance value (≈40Ω) was added to show whether the motor is able to drive the PV panel. The weight could vary due to the modeling error and the wind disturbance.

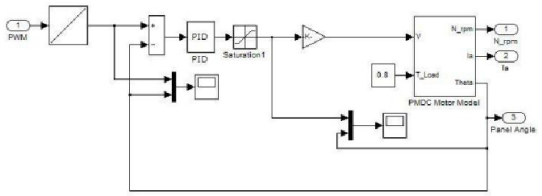

Fig.4 PMDC Motor Model

The panel current I_{pv} is used to charge the 12V battery. Simulation time is set to 36000 seconds corresponding to 10 hours (7am to 5pm).The sun angle and the panel angle is observed through the scope as this shows the actual tracker output

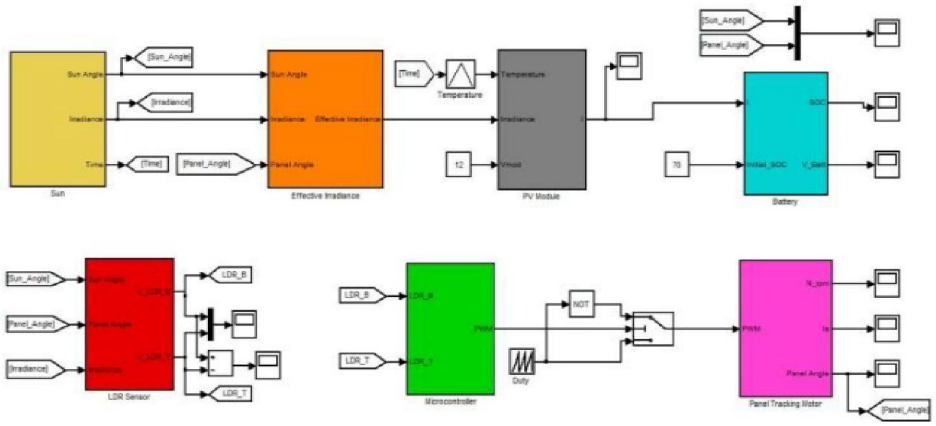

Fig.5 Smart PV Tracker Model

MODELING OF CEILING FAN PM BRUSHLESS MOTOR

BRUSHLESS DC MOTORS

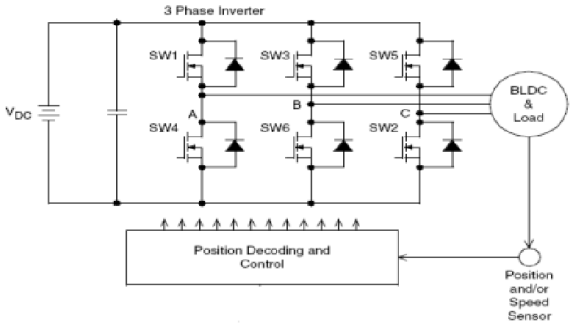

Fig.6 Basic Block Diagram of BLDC Motor

The Fig.6 illustrates the basic block diagram of BLDC motor. The controller logic circuits contain a binary state generator, which interprets the signals from the sensors and the input direction regarding the position of the permanent magnet rotor. The logic circuit outputs a code which tells a drive circuit, which windings should be energized. The rotation of the motor is changed within the control logic, which in turn reverses the phase energizing sequence. A switch or logic input is usually provided to convert the logic from clockwise to counterclockwise.

BLDC CEILING FAN MOTOR

Fig.7 Typical BLDC Ceiling Fan Motor

Today the typical ceiling fan is based on AC motors which are power hungry. Along with this the typical AC motor based fans have the rpm control through the capacitor or resistor based regulators and is not efficient as there is loss in the regulator itself to some extent. In addition the RPM control is by controlling the voltage and the voltage fluctuations of the mains make it very challenging to have constant RPM based on the AC mains supply. Further, existing AC motor solution, results in power factor degradation with no improvement for PF and there are other ill effects like harmonics injection to the AC mains, etc. The total amount of air flow or displacement is based on the blade size & rpm and does not change due to any other factor. The proposed solution is to keep the same air flow or displacement with less of energy usage along with improving the PF using the BLDC motor based ceiling fans. Typical BLDC motor based ceiling fan as shown in Fig.7 has much better efficiency and excellent constant RPM control as it operates out of fixed DC voltage. The proposed BLDC motor and the control electronics operates out of 12V DC. A comparison between BLDC and conventional ceiling fans is shown below (42" ceiling fan is considered). The power consumption is less than half at full speed and is about 20% at low speed for the BLDC motor compared to the conventional motor based ceiling fan, as can be seen from the Fig.8 below.

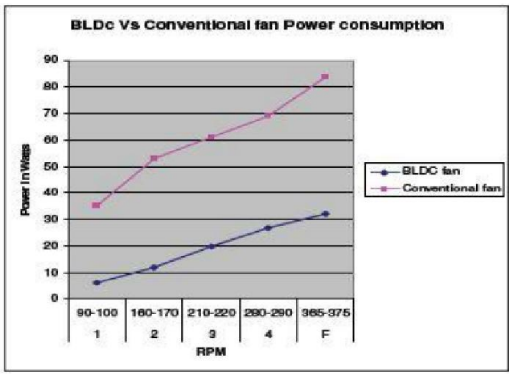

Fig.8 BLDC versus Conventional Fan Power Consumption

The mechanical energy required to rotate at full speed (typically 360rpm) for a 42" conventional ceiling fan is about 0.65Nm. The equivalent electrical energy would be around 26Watts, considering about 95% efficiency for mechanical to electrical energy conversion. The total power consumption of 32 watts as seen in the above design seems to be with in the design boundaries for such a motor.

MODELING OF BRUSHLESS MOTOR

The model of a BLDC consisting of three phases is explained by means of equations. Since there is no neutral used, the sum of the three phase currents must add up to zero (i.e.),

$ia+ib+ic=0$ (2)

$ia+ib=-ic$ (3)

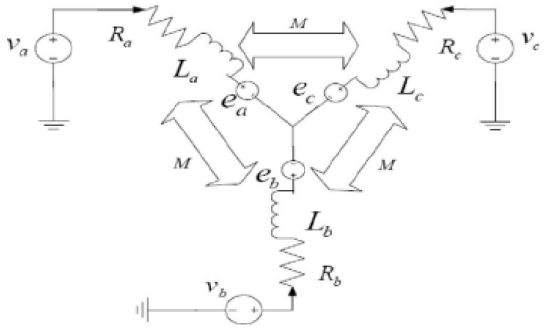

Fig.9 R, L and Back-emf BLDC Model

Referring to the Fig.9, the following equations are used to model the two pole three-phase BLDC motor.

$$\begin{bmatrix} v_a \\ v_b \\ v_c \end{bmatrix} = \begin{bmatrix} R_s & 0 & 0 \\ 0 & R_s & 0 \\ 0 & 0 & R_s \end{bmatrix} \begin{bmatrix} I_a \\ I_b \\ I_c \end{bmatrix} + p \begin{bmatrix} L_{aa} & L_{ab} & L_{ac} \\ L_{ba} & L_{bb} & L_{bc} \\ L_{ca} & L_{cb} & L_{cc} \end{bmatrix} \begin{bmatrix} I_a \\ I_b \\ I_c \end{bmatrix} + \begin{bmatrix} e_{as} \\ e_{bs} \\ e_{cs} \end{bmatrix} \quad (4)$$

If the permanent magnet inducing the rotor field is in the shape of an arc, it requires that the inductances be independent of the rotor position, hence

Laa=Lbb=Lcc=Lp (5)

Considering the symmetry of the above matrix in addition to independence w.r.t. the rotor position,

Lab=Lac=Lba=Lbc=Lca=Lcb=M (6)

Above equation reduces to

$$\begin{bmatrix} v_a \\ v_b \\ v_c \end{bmatrix} = \begin{bmatrix} R_s & 0 & 0 \\ 0 & R_s & 0 \\ 0 & 0 & R_s \end{bmatrix} \begin{bmatrix} I_a \\ I_b \\ I_c \end{bmatrix} + p \begin{bmatrix} L_p & M & M \\ M & L_p & M \\ M & M & L_p \end{bmatrix} \begin{bmatrix} I_a \\ I_b \\ I_c \end{bmatrix} + \begin{bmatrix} e_{as} \\ e_{bs} \\ e_{cs} \end{bmatrix} \quad (7)$$

From the above equations, we have

$$\begin{bmatrix} v_a \\ v_b \\ v_c \end{bmatrix} = \begin{bmatrix} R_s & 0 & 0 \\ 0 & R_s & 0 \\ 0 & 0 & R_s \end{bmatrix} \begin{bmatrix} I_a \\ I_b \\ I_c \end{bmatrix} + p \begin{bmatrix} L_p-M & 0 & 0 \\ 0 & L_p-M & 0 \\ 0 & 0 & L_p-M \end{bmatrix} \begin{bmatrix} I_a \\ I_b \\ I_c \end{bmatrix} + \begin{bmatrix} e_{as} \\ e_{bs} \\ e_{cs} \end{bmatrix} \quad (8)$$

Rearranging the equations, we have obtained equations in a form suitable for simulation. Thus, the model of the BLDC reduces to that in Fig 10. The back-emf waveforms e_a, e_b & e_c are trapezoidal in nature and can be represented by either the Fourier Series or by Laplace Transforms.

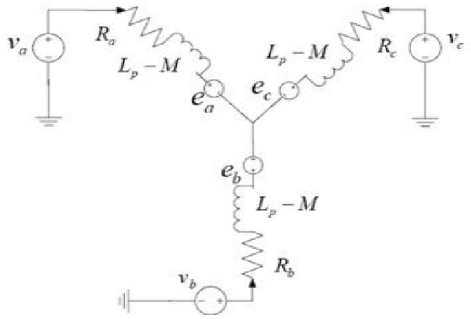

Fig.10 Simplified R, L and Back-emf BLDC Model

The back-emf is given by,

$$e_a = k_b f_{as}(\theta_r)\omega_m \quad (9)$$

where f_{as} is a unit function generator correspond to the trapezoidal induced emf as a function of rotor electrical positionθ_r. k_b is the emf constant and ω_m rotor electrical speed.f_{as} is given by,

$$\begin{aligned} f_{as}(\theta_r) &= (\theta_r)\ 6/\pi, && 0 < \theta_r < \pi/6 \\ &= 1, && \pi/6 < \theta_r < 5\pi/6 \\ &= (\pi - \theta_r)\ 6/\pi, && 5\pi/6 < \theta_r < 7\pi/6 \\ &= -1, && 7\pi/6 < \theta_r < 11\pi/6 \\ &= (\theta_r - 2\pi)6/\pi && 11\pi/6 < \theta_r < 2\pi \end{aligned} \quad (10)$$

The electromagnetic torque (Te) developed by the motor is given by,

$$Te = k_t\{f_{as}(\theta_r)i_a + f_{bs}(\theta_r)i_b + f_{cs}(\theta_r)i_c\} \quad (11)$$

$$Te = k_t \Phi_{as} I_a \quad (12)$$

The electromechanical equation with the load is given by,

$$Jp\omega_m + B\omega_m = (Te - T_L) \quad (13)$$

where J is the moment of inertia, B is the friction co-efficient and T_L is the load torque.

$$\omega_m = \int (Te - T_L - B\omega_m)/J \quad (14)$$

$$\theta_r = \int \omega_m dt \quad (15)$$

SPACE VECTOR MODULATION

For sinusoidal commutation, a sine lookup table has to be created with respect to the rotor angle. Space Vector Pulse Width Modulation (SVPWM) is a more sophisticated method to generate a fundamental sine wave that provides a higher voltage to the motor and lower total harmonic distortion (THD). The advantage of space vector PWM is, it considers the three phase inverter as a single unit.

For a three phase inverter shown in the Fig.6, there are 8 possible switching states. Among the 8 switching states, 6 states are active states and 2 states are zero states or null states. In active states, the motor terminals are connected to the DC bus through various combinations of the switches. During null states, the motor terminals are shorted through the upper or lower switches. The active states have the magnitude of $2V_{dc}/3$ which gives the hexagonal shape shown in the Fig.11.

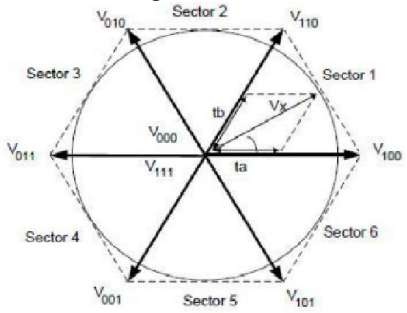

Fig.11 Space Vector Diagram

The possible eight switching states of an inverter is given in the Table 1.

TABLE 1 INVERTER SWITCHING STATES

State	ON Devices	V_{an}	V_{bn}	V_{cn}	Space Voltage Vector
0	S_2, S_4, S_6	0	0	0	V_0 (000)
1	S_1, S_4, S_6	$2V_{dc}/3$	$-V_{dc}/3$	$-V_{dc}/3$	V_1 (100)
2	S_1, S_3, S_6	$V_{dc}/3$	$V_{dc}/3$	$-2V_{dc}/3$	V_2 (110)
3	S_3, S_2, S_6	$-V_{dc}/3$	$2V_{dc}/3$	$-V_{dc}/3$	V_3 (010)
4	S_2, S_3, S_5	$-2V_{dc}/3$	$V_{dc}/3$	$V_{dc}/3$	V_4 (011)
5	S_2, S_4, S_5	$-V_{dc}/3$	$-V_{dc}/3$	$2V_{dc}/3$	V_5 (001)
6	S_1, S_4, S_5	$V_{dc}/3$	$-2V_{dc}/3$	$V_{dc}/3$	V_6 (101)
7	S_1, S_3, S_5	0	0	0	V_7 (111)

The locus of pure sinusoidal voltage waveform is circular in nature. Hence for the reference sine wave generation, each desired position on the circular locus is obtained by an average relationship between two neighboring active vectors. For the remaining time period, null vectors are used. For example, if the reference vector V_x is in sector 1 as shown in Fig.11, it can be resolved as,

$$V_x \cdot \sin\left(\frac{\pi}{3} - \alpha\right) = V_a \cdot \sin\frac{\pi}{3} \quad (16)$$

$$V_x \cdot \sin\alpha = V_b \cdot \sin\frac{\pi}{3} \quad (17)$$

Therefore,

$$V_a = \frac{2}{\sqrt{3}} \cdot V_x \cdot \sin\left(\frac{\pi}{3} - \alpha\right) \quad (18)$$

$$V_b = \frac{2}{\sqrt{3}} \cdot V_x \cdot \sin\alpha \quad (19)$$

where V_a and V_b are the adjacent vectors V_{100} and V_{110} respectively. Hence the reference vector V_x can be obtained by applying Va for the time t_a and V_b for the time t_b over a period T_0. The vector V_x is given mathematically as,

$$V_x = V_a + V_b = V_{100} \cdot \frac{t_a}{T_0} + V_{110} \cdot \frac{t_b}{T_0} + (V_{000} + V_{111}) \cdot \frac{t_0}{T_0} \quad (20)$$

Where, $t_a = \frac{V_a}{V_{100}} \cdot T_0$, $t_b = \frac{V_b}{V_{110}} \cdot T_0$,

$t_0 = T_0(1 - t_a - t_b)$.

The Simulink model for the ceiling fan brushless motor is shown below in Fig.12. Field oriented closed loop control technique with space vector modulation for the three phase inverter switches is incorporated.

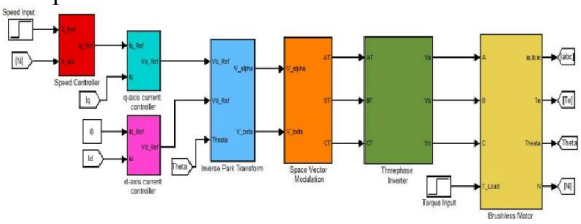

Fig.12 Ceiling Fan Model

The nominal speed and load torque of ceiling fan are 350RPM and 0.6Nm respectively. The ceiling fan motor parameters are shown in Table 2 below.

TABLE 2 CEILING FAN MOTOR PARAMETERS

Parameter	Value
Stator resistance per phase (R_s)	0.475 Ω
D-axis inductance per phase (L_d)	$8.5e^{-4}$ H
Q-axis inductance per phase (L_q)	$8.5e^{-4}$ H
Back-emf Constant (K_b)	15.966 V/s/rad
Torque Constant (K_t)	15.966 Nm/A
Moment of Inertia (J)	0.0008 $kg.m^2$
Co-efficient of Friction (B)	0.001Nm.s

SIMULATION RESULTS AND DISCUSSION

SMART PV TRACKER RESULTS

As per the modeling guidelines, the smart PV tracker is modeled in Simulink as shown in Fig.5. The panel current I_{pv} is used to charge the 12V battery. Simulation time is set to 36000 seconds corresponding to 10 hours (7am to 5pm).The sun angle and the panel angle is observed through the scope as this shows the actual tracker output.

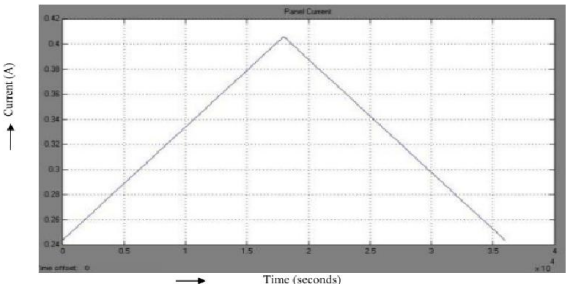

Fig.13 Panel Current

The above figure shows the panel current waveform. From the above figure it is clear that the maximum panel current is observed when the sun is perpendicular to the whole panel area (i.e., 12 pm noon). The peak value of the panel current indicates the high irradiance of sun during noon.

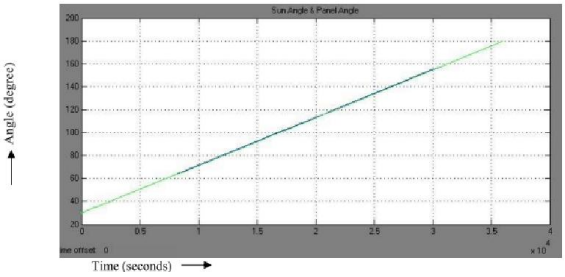

Fig.14 Sun Angle and Panel Angle

The above waveform gives the comparison of the sun angle with that of the panel angle. From the figure it is clear that the panel tracks the sun's movement at various irradiance. From Fig.14 it is observed that the panel angle follows the sun angle throughout 180 degree for all insolation.

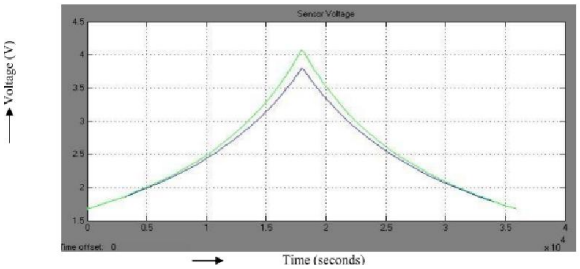

Fig.15 LDR Sensor Output

The above figure represents the output of the both top and bottom LDR sensors. The maximum difference between the two outputs is observed again at noon (12 pm)

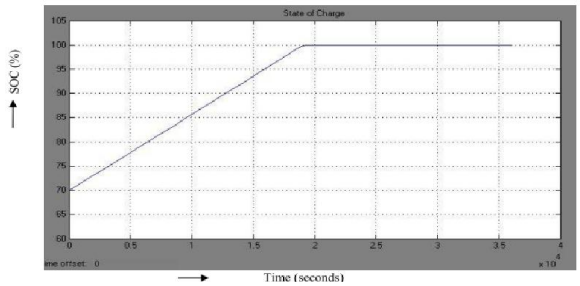

Fig.16 State of Charge of Battery

The above figure represents the state of charge of the battery. It takes nearly 5 hours for the battery to attain its 100% SOC by getting charged by the panel.

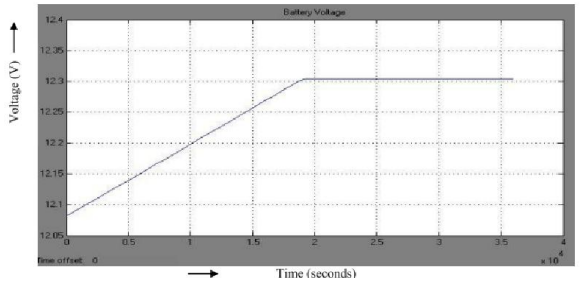

Fig.17 Battery Voltage

From the above figure Fig.16 it is observed that full charge represents 12.32V (100%). Also the complete discharge corresponds to 11.52V (0%).

CEILING FAN PM BRUSHLESS MOTOR RESULTS

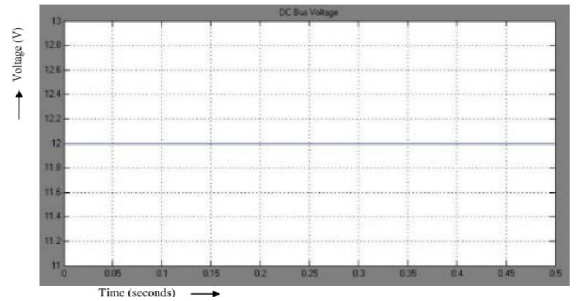

Fig 18 DC Bus Voltage

The above figure represents the12 V DC Voltage input for the BLDC Ceiling Fan motor which is coming out from the panel. It is fed to the three phase inverter.

The above figure represents the torque demand input variation to the ceiling fan motor. This is done to ensure the system response and stability. 0.5Nm torque corresponds to the load to the motor with blades connected. By varying the torque the response

of the system is observed by observing the variations in the other parameters such as speed, current and rotor angle.

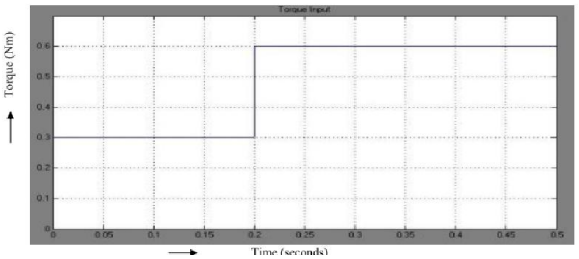

Fig.19 Torque Input

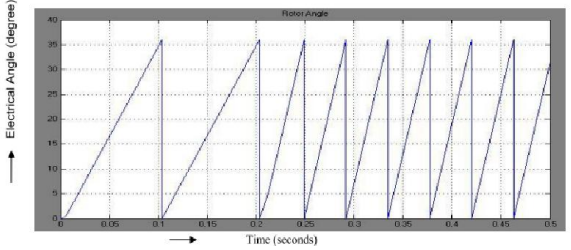

Fig.20 Rotor Angle

The above figure corresponds to the rotor angle of ceiling fan motor. As we are varying the torque an speed simultaneously, the corresponding response by the rotor is observed by variations in attaining its maximum value.

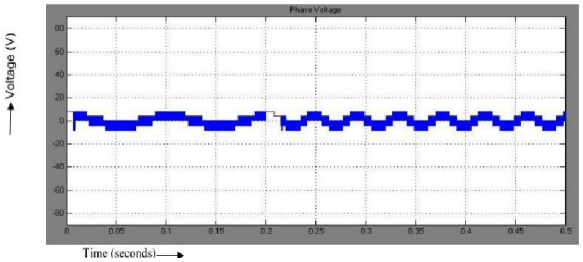

Fig.21 Phase 'A' Voltage

The above figure corresponds to the voltage waveform of the phase 'A'. It corresponds to the space vector pulse width modulated output of the DC input voltage(12V). From the above waveform itself it is clear that the maximum value of the phase voltage is 1.732($\sqrt{3}$) times that of the DC input voltage.

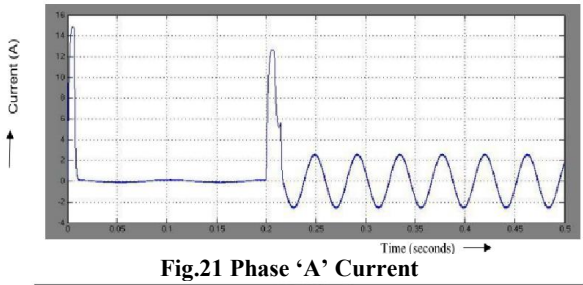

Fig.21 Phase 'A' Current

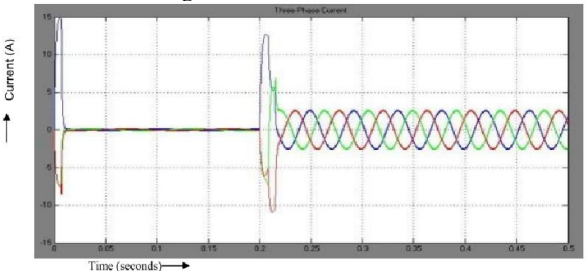

Fig.22 Three-phase Current

From Fig.21and Fig.22 it is observed that there is an increase in current to a high value as the motor starts with initial load and also due to the consecutive changes in input. It settles as the motor gains the speed.

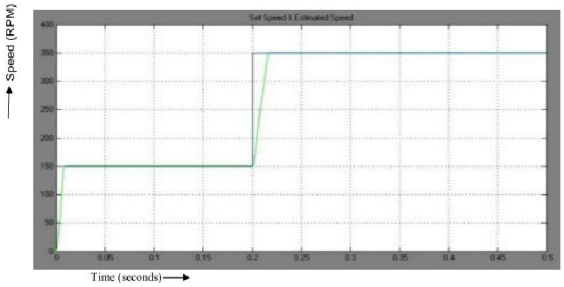

Fig.23 Speed Output

The above waveforms are the simulation results obtained from the ceiling fan brushless motor model in Simulink. Simulation time is set to 0.5 seconds. The torque input 0.6Nm is given in steps as shown in Fig.19. Coordinate transforms such as Clarke, Park, inverse Park and inverse Clarke are done to convert the three phase to two phase quantities and vice versa. Set speed and estimated speed of the fan motor is shown in Fig.23 and the control is much précised based on the waveforms observed.

CONCLUSION

In this work modeling of the smart PV tracker fed PM brushless motor for residential application i.e., ceiling fan has been presented. To extract the maximum power from the PV source single axis active solar tracker is used. The maximum output thus obtained from the panel is stored in the battery and it is fed to the brushless ceiling fan motor model. Field oriented control with sinusoidal space vector modulation technique is incorporated in the model to obtain highly précised control.

REFERENCES

1. C. Saravanan, Dr M.A. Panneerselvam, I. William Christopher, 2011, "A Novel Low Cost Automatic Solar Tracking System", International Journal of Computer Applications (0975 – 8887) Volume 31– No.9.
2. B. Koyuncu, K. Balasubramanian, 1991, "A microprocessor controlled automatic sun tracker", IEEE Transactions on Consumer Electronics.37, 913-917.
3. A. Zeroual, M. Raoufi, M. Ankrim, A. J. Wilkinson, 1998, "Design and construction of a closed loop sun-tracker with microprocessor management", Solar Energy. 19, 263-274.
4. P. Hatfield, 2006, "Low cost solar tracker", Bachelor of Electrical Engineering Thesis, Department of Electrical and Computer Engineering, Curtin University of Technology.
5. O. Bingol, A. O. Altintas, 2006, "Microcontroller based solar-tracking system and its implementation", Journal of Engineering Sciences.12, 243-248.
6. S. A. Kalogirou, 1996, "Design and construction of a one-axis sun-tracking", Solar Energy.57, 465-469.
7. H. Mousazadeh, A. Keyhani, A. Javadi, H. Mobli, K. Abrinia, A. Sharifi, 2009 , "A review of principle and sun-tracking methods for maximizing solar systems output", Renewable and Sustainable Energy Reviews. 13, 1800-1818.
8. [8] H. L. Tsai, 2010, "Insolation-oriented model of photovoltaic module using Matlab/Simulink", Solar Energy. 84, 1318-1326.
9. Tanvir Arafat Khan Md., S.M. Shahrear Tanzil, Rifat Rahman, S M Shafiul Alam, 2010, "Design and Construction of an Automatic Solar Tracking System", presented at 6th International Conference on Electrical and Computer Engineering, ICECE 2010, 18-20.
10. Jiping Chen, Tao Yu, Guanhua Zhou, Xingfeng Chen, Guolin Yu, 2011, "Design of the Attitude Automatic Adjusting System for the Solar Panel", presented at 2nd International Conference on Computing, Control and Industrial Engineering (CCIE), IEEE, pp 367 – 370.
11. Pillay P and Krishnan R, 1988, "Modeling of Permanent Magnet Motor Drives", IEEE Transactions on IA, vol.25, pp.274-279